Sylvain Martel, Ouajdi Felfoul, Jean-Baptiste Mathieu, Arnaud Chanu, Samer Tamaz, Mahmood Mohammadi, Martin Mankewich, Nasr Tabatabaei

NanoRobotics Laboratory
Department of Computer and Software Engineering,
Institute of Biomedical Engineering
École Polytechnique de Montréal (EPM)
Campus of the Université de Montréal
P.O. Box 6079, Station Centre-ville
Montréal (Québec), Canada H3C 3A7

sylvain.martel@polymtl.ca
www.nano.polymtl.ca

MRI-based Medical Nanorobotic Platform for the Control of Magnetic Nanoparticles and Flagellated Bacteria for Target Interventions in Human Capillaries

Abstract

Medical nanorobotics exploits nanometer-scale components and phenomena with robotics to provide new medical diagnostic and interventional tools. Here, the architecture and main specifications of a novel medical interventional platform based on nanorobotics and nanomedicine, and suited to target regions inaccessible to catheterization are described. The robotic platform uses magnetic resonance imaging (MRI) for feeding back information to a controller responsible for the real-time control and navigation along pre-planned paths in the blood vessels of untethered magnetic carriers, nanorobots, and/or magnetotactic bacteria (MTB) loaded with sensory or therapeutic agents acting like a wireless robotic arm, manipulator, or other extensions necessary to perform specific remote tasks. Unlike known magnetic targeting methods, the present platform allows us to reach locations deep in the human body while enhancing targeting efficacy using real-time navigational or trajectory control. The paper describes several versions of the platform upgraded through additional software and hardware modules allowing enhanced targeting efficacy and operations in very difficult locations such as tumoral lesions only accessible through complex microvasculature networks.

KEY WORDS – Nanorobots, bacteria, medical robotics, MRI, target chemotherapy, blood vessels

1. Introduction

Because of the success rate coupled with lower morbidity compared to traditional open surgeries, the number of image-guided endovascular interventions being performed each year is increasing. During such interventions, a small diameter metal wire referred to as a guidewire is first inserted (Seldinger 1953). Such guidewire having a highly flexible tip with hydrophilic coating is used to provide a stable rigid track for the insertion of a flexible catheter introduced over the wire. This technique allows catheterization of almost any blood vessel down to a few millimeters in diameter. But many types of medical interventions are still out of reach to catheterization, in particular the ones that must target regions in the human body only accessible through smaller diameter vessels. Among many possible interventions out of reach to catheterization, tumor targeting including target chemotherapy and chemo-embolization are of special interest due to the high number of patients diagnosed with cancer while offering the advantages of improved concentration of therapeutic agents at the targeted area and a decrease of systemic side effects compared to traditional chemotherapy-based interventions (Alexiou et al. 2005).

These targeted regions are accessible by transiting through anarchic arteriocapillar networks stimulated by tumoral angiogenesis with capillaries located near the target as small as 4-5µm in diameter. As such, the popularity of magnetic nanoparticles as carriers for therapeutic agents for target interventions in cancer therapy, have been increasing during the recent years. Indeed, magnetic nanoparticles have unique properties for this type of interventions. First, they can be manipulated by an external magnetic field gradient. Second, they disrupt the local magnetic field creating a net field inhomogeneity that can be picked up as a negative contrast (local decrease in image intensity) in T_2-weighed magnetic resonance imaging (MRI) which is essential for monitoring and closed-loop navigation or trajectory control within a robotic platform. Third, they can generate heat when exposed to an alternating magnetic field which can be used as hyperthermic agents to destroy tumor tissue, or as a computer-triggering mechanism to release drugs from polymeric carriers containing magnetic nanoparticles while elevating the temperature locally for achieving enhanced therapeutic results.

Present implementations for targeting tumors rely on an external permanent or an electro-magnet located near and above the tumor, e.g. (Driscoll et al. 1984; Alexiou et al. 2000). A catheter is typically used to release the magnetic nanoparticles as close as possible to the target. But because of higher field intensity towards the external magnet, e.g. (Alexiou et al. 2006), targeting is mostly restricted to tumors near the skin with significant reduction of targeting efficacy as the targets get deeper in the body. Furthermore, since the approach relies on trapping the particles without navigation or trajectory control over pre-planned paths, the distance between the releasing site and the tumor significantly affects

targeting effectiveness. Indeed, the reachable limits of catheterization combined with complex microvasculature networks contribute to lower significantly targeting performance further.

Hence, as minimum requirements, an efficient interventional platform for tumor targeting or for other operations in the human microvasculature must not only be able to manipulate magnetic carriers in a 3D volume but also provide an integrated imaging modality allowing effective navigation along pre-planned paths through real-time closed-loop control from the catheterization boundaries to specific targets such as tumoral lesions. As such, this paper proposes and describes a medical robotic platform with upgraded versions providing enhanced performance through additional software/hardware subsystems suited for medical interventions in the microvasculature.

2. MRI System Upgraded with Software Only – Level 1 Platform

2.1. Basic Principles and Proof of Concept

Upgrading a clinical MRI system with software only is the least expensive approach to convert a platform that has been used so far for diagnostic purposes only to an effective interventional platform (Martel et al. 2004). The feasibility of controlling the displacement of an untethered object such as a carrier or a nanorobot[1] in the blood vessels of a living animal has been demonstrated for the first time in (Martel et al. 2007a) using a special medical protocol described in (Martel et al. 2007b) with a description of the interaction between the various components required for medical interventions in (Martel 2007). In this particular demonstration being part of a project known as MR-Sub (Magnetic Resonance Submarine), a ferromagnetic bead was navigated in real-time and without human interventions along pre-planned trajectories in the carotid artery of a living swine at an average velocity of 10 cm/s. Here, propulsion force was induced from a technique developed by our group and referred to as magnetic resonance propulsion (MRP) which has been described in more details in (Mathieu et al. 2006). While tracking the object being controlled, MRP was used in a time-multiplexed fashion (Fig. 1) and generated from the same three orthogonal imaging gradient coils (used for MR-imaging slice selection) already implemented in clinical MRI platforms.

The experiment confirmed that a clinical MRI system can provide the three essential components for real-time controlled navigation of untethered devices or robots in the human vasculature namely, propulsion, tracking, and closed-loop control. Propulsion used the conventional MR-imaging gradient coils combined with additional specialized software modules integrated onto the platform while imaging used the same hardware and software already available from the MRI

platform. Tracking used the same conventional hardware already found in conventional MRI systems while using a special tracking algorithm developed by our group (Felfoul et al. 2008). Combined together through a special software architecture (Fig. 2) with new modules (Chanu et al. 2008) connected to a user's interface (Fig. 3), resulted in real-time closed-loop control (Tamaz et al. 2008) to be executed on the same MRI computing system which was linked to embedded communication ports that allowed commands to be sent through propulsion gradients based on previous tracking information.
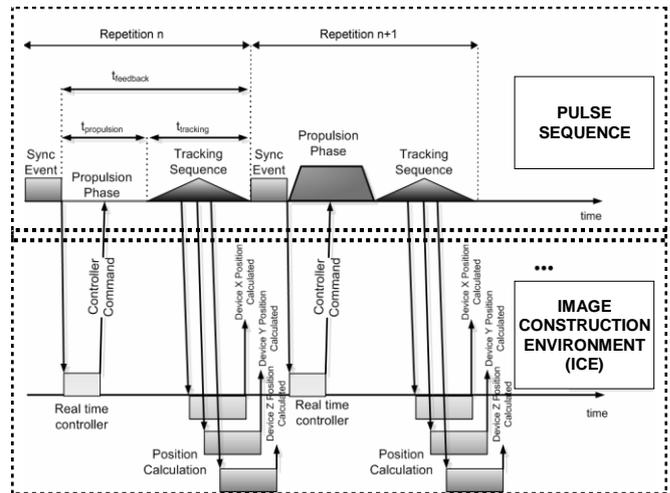

Fig. 1 Representation of the basic sequence of events used within the environment of the MRI platform for the closed-loop displacement control of wireless entities along pre-planned paths in blood vessels.
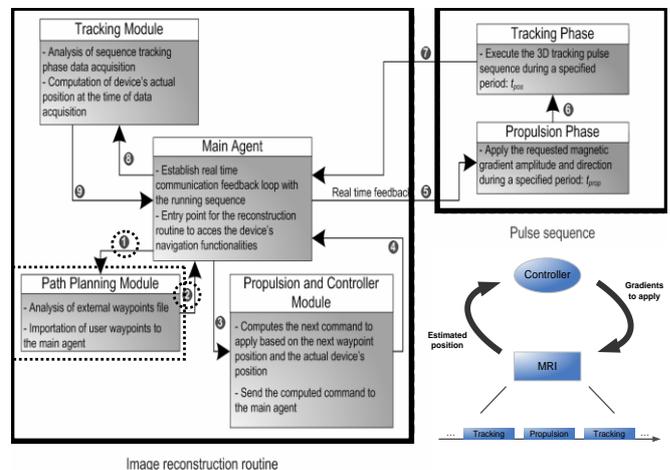

Fig. 2 Basic block diagram representing the software architecture for MRP-based applications with the main software modules and communication paths sequentially numbered. Paths and module surrounded by a dotted shape are executed only once unlike other paths and modules being called at a typical minimum frequency of 24 Hz.

---

[1] A nanorobot is defined here as a micro-entity operating under feedback control and relying on parts < 100nm (approx.) used to implement new embedded functionalities.
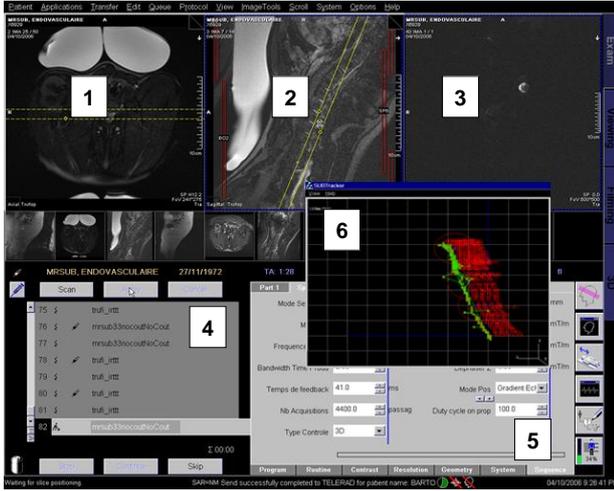
Fig. 3 User interface as seen on a computer display during MRP-based operations showing some of the main windows (other windows used for trajectory path planning through waypoints and signal quality verification (SNR), etc., are not shown): (1) and (2) provide high-resolution MR-images inside the body (here a living swine) for adequate placement of the body within the MRI bore; (3) is used for magnetic compatibility check required to ensure that no other magnetic objects besides the ones being controlled are in proximity; (4) and (5) are being part of the sequence editor; and the displacement of the untethered ferromagnetic core based on MR-tracking information is being displayed in (6).

2.2. MRI as Imaging Modality

The use of MRI as imaging modality for such applications has many advantages which also explain its recent emergence as an alternative to digital subtraction angiography (DSA) of image-guidance of endovascular procedures, where angiography is well known as a medical imaging technique used to visualize the inner structure of blood filled structures. At comparable temporal resolution which is a key specification when operating under real-time constraints, MRI allows visualization of soft tissue anatomy not possible with projection x-ray image. Soft tissue visualization although useful in medical applications such as stroke therapy, aneurism coiling, angioplasty, and myocardial stem cell delivery, may also prove to be essential in our target diagnostic and therapeutic applications where information about the vessel wall and tissue surrounding blood vessels in real-time may be important. Other advantages of considering MRI as an imaging modality also include the lack of nephrotoxicity associated with iodinated contrast media used in DSA (Bettman et al. 1997), and absence of ionizing radiation exposure for the patient or the medical staff. Beyond these advantages and the fact that MRI platforms are already available in most clinics, MRI is also sensitive to a variety of physical parameters that can be used as contrast mechanisms (Li et al. 1999; Li et al. 2002; Louie et al. 2000; Josephson et al. 2001; Lowe et al. 2001; Meade et al. 2003) providing physiological and metabolic data combined with physiological information.

Compared to another recently proposed interventional platform relying on an untethered magnetically driven sensor where line of sight is used for feeding back tracking information (Ergeneman et al. 2008), the use and tight integration of MRI to gather tracking information and allowing operations deep in the human body where line of sight is not possible represent one of the main particularities and advantages of this proposed method and platform.

2.3. Main Limitations of Using Additional Software Only

The use of MRI systems for implementing new medical robotic platforms imposes some serious constraints due to the fact that MRI systems were initially developed as an imaging or diagnostic equipment. As such, one major difficulty was and remains the implementation of additional specialized modules within the constraints of a software architecture initially dedicated to MR-imaging only while maintaining real-time performance. For instance, delays in communication and interaction between various modules add latencies which must be managed to guarantee stability during feedback control actions (Tamaz et al. 2008). Another important drawback is the limited maximum gradient (typically in the order 40mT) that can be generated by each of the three orthogonal coils in a conventional clinical MRI system which constrains the maximum reachable MRP level.

Indeed, the induced force (Eq. 1) produced by magnetic gradients and acting on a ferromagnetic core with a volume V within an untethered biosensor, carrier, or robot depends on the MRP duty cycle R and the magnetization of the core material which reaches saturation level (Msat) when placed in the bore or tunnel of a 1.5T or higher field MRI system, is computed according to

$$\vec{F} = R \cdot V (\vec{M} \cdot \nabla) \vec{B}. \tag{1}$$

In turn, previous experiments performed by our group showed that the gradient coils of clinical MRI systems tend to overheat and as such, the time dedicated to MRP must often be reduced appropriately to allow for cooling, hence affecting the induced force through a reduction of the duty cycle R which can be further reduced by the image or tracking acquisition time.

2.4. Solutions to Increase Performance

We also estimated (Mathieu et al. 2006) that the hydrodynamic diameter d_h of each particle, carrier or robot must be approximately half the diameter of the blood vessel being navigated providing the best trade-off between the volume dedicated to embedding magnetic material for induced MRP force versus the added negative effects on displacement caused by the vessel walls, a phenomenon described in (Fidleris and Whitmore, 1961). Hence, for target chemotherapy, the d_h of each loaded particle within an agglomeration could be as small as 2μm whereas for target chemo-embolization, a $d_h \approx 20$μm or even slightly larger could provide in some cases (although further studies are required to confirm it), beneficial therapeutic efficacy by being retained at the entrance of smaller diameter vessels at

locations sufficiently close to the tumoral lesion. At such sizes, considering that the volume dedicated to magnetic material must be smaller than the overall volume of the devices or objects being propelled to allow room for loading therapeutic agents, suggests that the gradient provided through a MRI system being only upgraded by software may yield limited performance for efficient targeting when operating in the microvasculature. Indeed, the corresponding magnetophoretic velocity of a single object in a fluid with viscosity η in the absence of blood flow (with a vessel diameter sufficiently large such that wall effect can be neglected) can be expressed as

$$\vec{v} = \frac{1}{3\pi\eta d_h}\vec{F}\cdot \tag{2}$$

Such velocity must be sufficient to steer adequately the particles towards desired directions at vessel bifurcations which typically occur in the presence of blood flow and perturbations.

But some options are available to maximize directional control using a MRI platform upgraded only with software. One option is to use a balloon catheter in larger diameter vessels or larger magnetic embolization carriers in smaller vessels to reduce blood flow temporary allowing more effective steering to be performed. Another option that can be used in combination to the latter is to increase the magnetization saturation of the core material. As such, conventional biocompatible Magnetite (Fe_3O_4) can be replaced by Iron-Cobalt (FeCo) providing four times the magnetic force density if the issue of convincing the medical community while synthesizing the cores to prevent toxic Cobalt ions to come in contact with blood can be resolved. Nonetheless, although it is possible without hardware modifications to navigate a ferromagnetic core beyond the reach of catheterization allowing new opportunities due to a larger possible targeting region in the human body, the limited magnetic force due to the relatively low gradients provided by conventional MRI systems still prevent its efficient use in the microvasculature. Therefore, for operations in such more demanding targeted regions, an upgraded MRI-based version of the system relying on special gradient coils becomes highly suitable.

3. MRI System Upgraded with Additional Steering Gradient Coils (SGC) – Level 2 Platform

3.1. Gradient Strengths

In (Mykhaylyk et al. 2005), it was shown that several T/m gradients were necessary for efficient attraction of Magnetite nanoparticles in mice blood vessels. The generation of such gradients for navigation in the blood vessels may be feasible for small animals but technological constraints will most likely prevent the implementation of such high gradient coils (with sufficient switching frequencies and within FDA recommendations) within the space constraints imposed by

the bore of clinical MRI machines when operating on larger animals including humans.

But previous studies and experiments performed by our group (Mathieu and Martel, 2007) showed that gradients in the 100-500mT range representing only one order of magnitude increase compared to standard MRI gradient amplitudes could be sufficient for targeting tumors through the microvasculature when using microparticles instead of nanoparticles. In such a case, a higher effective V (Eq. 1) while retaining the advantages of using nanoparticles as described previously can be achieved by using polymeric microbeads ($d_h \geq 2\mu m$) encapsulating nanoparticles with a proper density to yield sufficient magnetic force and distributed in a way as to maintain the advantages and possibilities including local hyperthermia associated with the use of nanoparticles as described earlier in this paper. Also as stated earlier, single magnetic domain nanoparticles prevent MR-image distortion while being traceable like MRI contrast agents.

The additional steering gradient coils (SGC) required for these highly demanding applications can be implemented from two types of configurations referred here to as PS and TIPS coils as described in the next two sections.

3.2. Dedicated Propulsion/Steering (PS) Coils

A new set of coils dedicated to propulsion and/or steering (e.g. when blood flow is used for propulsion as it is the case in smaller diameter blood vessels especially when d_h is smaller than the diameter of a red blood cell as in smaller capillaries) and referred here to as PS coils can be installed between the imaging gradient coils (IGC) and the center of the MRI bore.

PS coils do not need many of the stringent specifications required to guarantee the performance of MR-imaging coils, making their implementations easier in this respect. For instance, the performance of MRI gradient coils are typically measured with regard to coil efficiency often expressed as gradient per unit current, inductance, power dissipation, and gradient homogeneity. Unlike MRI coils, the latter is not as critical for PS coils but power dissipation and coils efficiency is an important consideration since relatively large gradients must be sustained.

Hence, a logical approach to implement such PS coils capable of generating higher gradient amplitudes is to increase the winding number within the space constraints in order to maintain the electrical current below an acceptable threshold. This will be done at the expense of larger inductance in the coils yielding an increase of the gradient rise time that fortunately may be tolerated up to a certain threshold. Indeed, due to proton relaxation time, MR-imaging gradient coils must provide a total rise time as short as 200μs requiring low inductance in the coils, but the rise time of PS coils can be much longer (in the order of milliseconds) since induced force begins or continues to be effective during transition time (rise and fall time) while the maximum PS rate remains much lower compared to fast MRI sequences.

3.3. Tracking/Imaging/Propulsion/Steering (TIPS) Coils

One of the major limitations for generating high gradients is the heat dissipation of the gradient coils. Adding orthogonal PS coils next to the MR-imaging coils may represent simpler design challenges as explained in the preceding section but the total volume available for its implementation while allowing for adequate heat dissipation is relatively small especially when enough room must be maintained in the MRI bore to place a large animal or an adult size human.

As such, one alternative is to replace a configuration based on separate MR-imaging and PS coils by one relying on one set of orthogonal coils capable of tracking, imaging, propulsion, and steering (TIPS) in a time-multiplexed fashion between (T or I) and (P or S). Although the implementation of the TIPS coils would benefice from extra volume provided by the removal of the MR-imaging coils, the design of such coils become more stringent and challenging since they must be capable of short rise time, high gradient homogeneity, and high gradient amplitudes. At present, although superconductive TIPS coils are being considered by our group, it is still unlike PS coils, a theoretical concept requiring further investigations.

4. MRI System Upgraded with Additional Steering Magnetic Coils (SMC) – Level 3 Platform

4.1. Bacterial Carriers, Sensors, and Robots

In some instances, particularly in very small capillaries, the flagellated motor in bacteria could help achieving enhanced targeting when maintaining a sufficiently high duty cycle with high gradient amplitudes for MRP cannot be achieved. In (Martel 2005; Martel 2006a), the use and integration of bacteria and more specifically magnetotactic bacteria (MTB) as means of actuation, propulsion and steering for small objects including micro- and nanorobots (project MTBot) has been proposed and described while recognizing their potential for applications in the human blood vessels (Martel 2006b). The latter has been proposed based mainly on the appropriate diameter of the cell of the MC-1 MTB (~2μm being approximately half the diameter of the smallest capillaries in human), encouraging first set of tests showing potential for full biocompatibility, and measured thrust force provided by each MC-1 MTB exceeding 4pN which knowing present technological constraints, identified such bacteria as serious bio-actuators to be considered for operations in the microvasculature. Recently, experimental results published in (Martel et al. 2006) showed that a single bacterium operating under computer control could be used to propel and steer accurately a micrometer-scale object (that could also be a biosensor, carrier, or a micro- nanorobot), in this particular case being a 3μm bead, along a pre-planned path. Although later, chemical- (Behkem and Sitti 2007) and phototaxis-based (Steager et al. 2007) stop/resume motion control of bacteria have been reported, both cases failed to demonstrate steering control.

Steering control while maintaining maximum velocity of the bacteria (although we also showed that the velocity of MTB can be controlled by magnetic field intensities, an approach more suitable when operating in environments such as the human vascular network) is considered the most important requirement for bacterial carriers or robots especially the ones dedicated to this type of applications. The use of the MC-1 MTB in our experiments not only showed that steering control can be implemented in a dedicated computer software module, but also that the velocity achieved when pushing a bead with similar characteristics was at least one order of magnitude higher (while retaining the possibility of moving larger objects with larger quantities of bacteria) compared to other studies having no steering control. By being non-pathogen, the lifespan of these bacteria in the human body is limited and as such, a higher swimming speed means longer distances with potentially better targeting especially in very complex microvasculature networks. Furthermore, for various reasons, this type of medical procedures making use of relatively expensive platforms and personnel must have the shortest possible interventional time which demands for higher displacement speeds.

Another concept worth mentioning in this context is the replacement of the flagella of the bacteria such as the ones being used for the implementations of our bacterial carriers by artificial flagella in the form of nanocoils (Bell et al. 2007) being propelled with the use of a rotating magnetic field, a method previously mentioned in (Honda et al. 1999). Although the maximum velocity was much inferior than what has been achieved with MTB (~4.6μm/s vs. ~300μm/s), the principle is still quite attractive for various reasons (extended operational life, non-biological nature of the system, etc.) but could be extremely difficult if possible to implement in the bore of an MRI machine. But this fact also holds true for the MTB-tagged carriers. For the former, the high intensity DC magnetic field (typically 1.5 or 3T) of the clinical MRI machine would maintain the nanocoils oriented towards a constant direction (without the possibility of re-orientation) preventing efficient navigation in blood vessels not perfectly aligned with the initial alignment of the nanocoils, which is a critical issue especially in complex vasculatures. For the latter, our preliminary experimental results suggest that the swimming speed of MTB-tagged carriers will be null when inside a 1.5T or higher DC field. Furthermore, since the directional control of MTB is based on magnetotaxis where the orientation of the MTB-tagged carriers can be changed by inducing a torque on a chain of nanoparticles called magnetosomes embedded in the cell of each bacterium from a low intensity directional magnetic field, the presence of a high DC magnetic field would prevent an adequate implementation of this method. Hence, the directional or steering magnetic coils (SMC) used to influence and control the swimming direction of these bacteria should be implemented outside and next to the MRI bore where the intensity of the DC magnetic field is sufficiently low.

4.2. SMC Main Specifications

Compared to a purely synthetic approach such as the nanocoils mentioned in the preceding section, a hybrid approach where synthetic and biological components are integrated in the same system may provide in many instances some significant advantages. Indeed, the use of MTB means that no electrical power is required for propulsion but for directional control only especially when maximum velocity of the MTB-tagged carriers is suitable.

The molecular motor embedded in flagellated bacteria measures approximately 270 nanometers (nm) across and has a rotor that can operate at 6,000 to 17,000 revolutions per minute (rpm) (200 to 1000 rpm with the flagella attached). Because this rotary engine is powered by a flow of protons, no source of electrical energy is required for propulsion. In our particular implementation, this means that no coils configuration is necessary for propelling MTB-tagged carriers, sensors, or robots but only coils dedicated to directional control, i.e. capable of generating sufficient torque to influence the orientation of the chain of magnetosomes embedded in each MTB. Even at a distance sufficient to allow operations in a human, the electrical power required for such operations is relatively very low considering the fact that our experimental data showed that accurate displacement control of these MTB is achieved with very low directional field slightly higher that the geomagnetic field of 0.5 Gauss (extremely low compared to the field required to propel and direct a synthetic core or object such as our ferromagnetic carriers or the nanocoils mentioned earlier).

This is quite significant since it allows unlike other synthetic-based implementations, a level of propulsion and steering in microvasculature deeply located in the human body that would otherwise be extremely challenging if feasible to realize if other technologies would be considered instead. We also found experimentally that with intensities slightly higher than 0.5 Gauss, that possible displacement errors along a pre-planned path caused by chemotaxis, aerotaxis, and others factors such as Brownian motion, become negligible compared to magnetotaxis. The other advantage of the orthogonal SMC configuration capable of 3D directional field generation is that other implementation issues such as power dissipation is not a real concern which is not necessary true for most other coils implementations where MTB are not considered.

5. MRI-based Nanorobotic Platform

A basic diagram of the hardware architecture of the MRI-based nanorobotic platform is depicted in Fig. 4. It consists of three main interventional positions denoted P1-P3 in Fig. 4. Sliding rails operated under computer control are used to transfer the table where the patient lies, at P1, P2 or P3.

At P1, a fluoroscopic system or a CT scanner is used during catheterization (being hard to achieve using MRI unless non-standard catheters are being used). The fluoroscopy system provides a source and detection of x-rays allowing projected images of the patient and arteries filled with a radio-contrast agent with the possibility of x-ray axial images of the patent obtained if a CT scanner is used instead. It should be noted that P1 and the associated system are optional for this platform but are highly suitable for interventional radiologists that are all typically experienced using x-ray as an imaging modality during catheterization.

Once catheterization is completed, the patient is moved to location P2 inside the bore of the MRI system where untethered entities such as magnetic carriers are released typically from the tip of the catheter. There, propulsion gradients calculated in the control consol in the computer displays section in Fig 4 are sent from the imaging gradient coils (IGC) through amplifier unit 1 (AU1) in the case of a level 1 platform (Sect. 2) or from the SGC coils (configured as PS or TIPS coils) through AU2 for a level 2 (Sect. 3) or level 3 (Sect. 4) platform.

Although a level 2 platform should be sufficient for interventions such as target chemo-embolization where larger untethered micro-entities hence containing more magnetic material are used, a level 3 platform may enhance efficacy for applications such as target chemotherapy where much smaller untethered micro-entities with much less magnetic material designed for the smallest capillaries including angiogenesis blood structures may prove to be difficult to steer using the SGC alone.
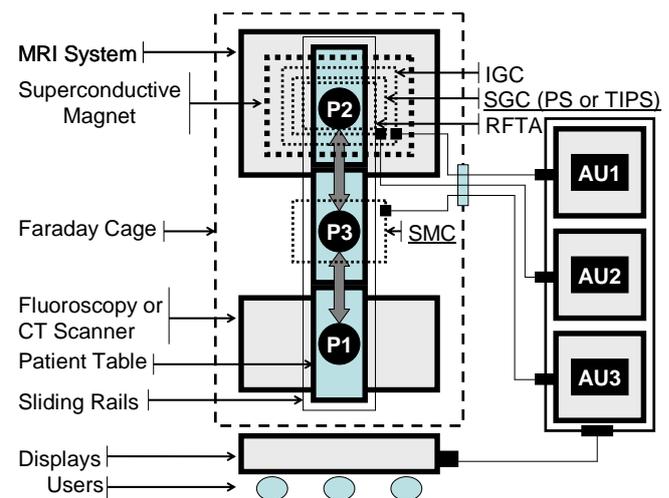

Fig. 4 Basic diagram of the proposed MRI-based nanorobotic interventional platform showing the various types of coils with the corresponding amplifier units (AU) where the names of the additional custom coils are shown underlined. At different stage of the operation, the patient can be positioned at three different sites within the platform namely, P1: initial operations under fluoroscopy or CT scan typically for catheter placements; P2: delivery in the MRI system of untethered ferromagnetic carriers after being released from a catheter; and P3: final targeting in the microvasculature including the tumoral lesion using MTB-tagged carriers.

Hence, an envisioned approach consists of the use of special ferromagnetic embolization carriers capable of encapsulating MTB-tagged carriers with a release mechanism relying on hyperthermic-based computer commands or a polymeric-based approach such as the synthesis of specific time-biodegradable polymers.

The distance between the SMC and the superconductive magnet of the MRI system must be far enough so that the influence of the B_0 field with typical maximum value of 1.5 or 3T can be compensated for inside the SMC configuration. Such distance along a center axis (x) for instance and corresponding to the rails longitudinal axis can be chosen by measuring the DC magnetic field intensity of the MRI machine and/or from graphics or layouts provided by the manufacturer representing the magnetic intensity distribution around the MRI platform. In all cases, one can match these values to an analytical expression (Hatch and Stelter 2001) estimating the field intensity along the center axis (x) of a magnet which is given by

$$B(x) = \frac{B_r}{\pi} \left[\tan^{-1}\left(\frac{x+1}{wt} \sqrt{t^2 + w^2 + (x+l)^2} \right) \right.$$
$$\left. - \tan^{-1}\left(\frac{x}{wt} \sqrt{t^2 + w^2 + x^2} \right) \right] \quad (3)$$

where l is the length of the magnet, w its width and t its thickness with B_r being the residual induction of the magnet, a characteristic of the material used.

It is obvious that the field intensity increases significantly within the SMC when the latter is located closer to the bore of the MRI system which can be suitable in the point of view of minimizing travelling delay of the patient between locations P2 and P3 when time-multiplexed sequences between controlling the displacement of MTB-tagged carriers at P3 and tracking their positions using MRI at P2 must be executed several times for enhanced targeting and monitoring purposes. Furthermore, although the use of a 3T MRI system instead of a 1.5T platform would allow better quality of imaging in a given time interval or shorter imaging acquisition time for a minimum acceptable quality of the image or information required to support the operation adequately, the distance between P2 and P3 would have to be extended causing additional travelling delay unless more compensation requiring more electrical energy is implemented in the SMC system. In other words, the location of each components of such a platform must be adequately chosen based upon specific characteristics of the units influencing neighboured systems while taking into account the types of medical protocols being envisioned.

All preceding units are enclosed in a faraday cage typically used to prevent RF transmissions generated by the RF transmitters and antenna (RFTA) assembly as depicted in Fig. 4, to escape. The IGC, SGC, and the SMC are connected and driven by AU1, AU2, and AU3 respectively which are located outside the faraday cage. Each amplifier unit controlled independently by computer would typically have different electrical specifications and cooling requirements. Computer displays with graphical user interfaces (GUI) similar to the one depicted in Fig. 3 are provided for all computerized functions required prior to and during each intervention.

6. Experimental Methods

Experiments were conducted to gather data under real physiological conditions in order to evaluate the capability of such MRI-based nanorobotic platform with different levels of performance configurations as described in the previous sections. Because of the differences between the different configurations, the methodology or protocol used to gather experimental data varied for each level as described in the following sections.

6.1. Method for Level 1 Platform Assessment

In vivo experiments were conducted on domestic pigs under general anesthesia in order to validate the platform for future operations in humans since the pig is known to be an animal model being very close to human. A 1.5mm (13.6mg) diameter chrome steel sphere was used initially to reduce the risk of failure during a relatively expensive and complex experiment conducted with a surgical team, while providing valid data to prove the concept and confirm our mathematical models. The saturation magnetization being reached when placed in the bore of the MRI system was 1.36×10^6 A/m and measured using a vibrating sample magnetometer (Applied Research Corp. model 155). A 7-F introducer was inserted into the artery using a standard interventional procedure under x-ray fluoroscopy (equivalent to P1 in Fig. 4). Once placed in the bore of a 1.5T Siemens Magnetom Avanto clinical MRI system (P2 in Fig. 4) only upgraded with our custom software modules (i.e. without any hardware modification or addition), a 3D angiogram with gadoteridol injection was acquired (Fig. 5a) to visualize the carotid artery. The MR-image was digitally filtered (Fig. 5b) to subtract any information that could confuse the software when controlling the displacement of the sphere along the pre-planned path. Then waypoints defining the path to be followed by the ferromagnetic bead inside the artery were added as depicted in Fig. 5c using a custom interface.

Then a 5-F GLIDECATCH catheter with the bead wedged on its tip was inserted into the introducer by an interventional radiologist. Due to large MR-image distortions caused by the ferromagnetic sphere (Fig. 5d) preventing accurate localization of the sphere, a new real-time MR-tracking algorithm developed by our group, named magnetic signature selective excitation (MS-SET) and integrated in our software architecture was used for tracking. This tracking method being used during the experiment, applied RF excitation signals tuned to the equipotential magnetic curves generated by the magnetic signature of the sphere being tracked. The 3D position of the ferromagnetic object was achieved with a correlation function performed on each k-space line of each of the three axes corresponding to the three projections necessary to determine the best possible accurate localization of the sphere within the time constraint required to guarantee stability of the feedback controller.

Once the bead was detected within the field of view (FOV) by the computer system (Fig. 5e and Fig. 5f), the bead was released and controlled without human intervention successively along the waypoints (Fig. 5g). MS-SET employed a modified Spin Echo (SE) rather than a Gradient Echo (GE) sequence to allow re-phasing of the excited spins.
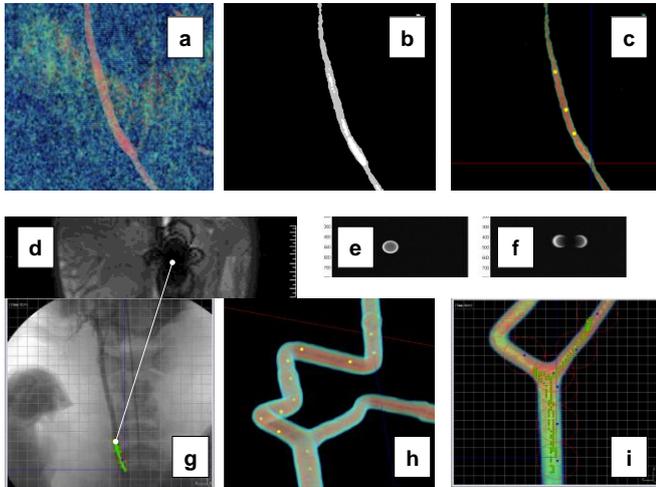

Fig. 5 Some MR-imaging techniques used for the experiments; (a) and (b) unfiltered and filtered MR-image of the carotid artery of the living animal; (c) the same artery with waypoints being plotted to provide trajectory control commands to the computer; (d) distorted MR-image created by the 1.5mm chrome steel sphere; (e) and (f) MR-image of the ferromagnetic sphere using the MS-SET method as seen in the transversal and sagittal plane respectively; (g) the same ferromagnetic sphere being tracked using the MS-SET method over a pre-acquired x-ray image (optional) providing additional physiological information (e.g. the spinal cord) while being controlled at 24 Hz in the carotid artery of the living swine along the waypoints (the line joining Fig. 5d shows the difference when using the MS-SET method compared to a distorted image); (h) shows the waypoints plotted over the MR-image of a phantom mimicking human vascular conditions and being showed through a dedicated imaging software with (i) the respective real-time displacement of the sphere being displayed.

Initially, a simple proportional-integral-derivative (PID) control function was implemented to evaluate the method with a well known yet simple controller prior to develop more advanced control algorithms better suited for such applications. To evaluate the technique in more complex human pathways in the presence of bifurcations, the same experiment was repeated in phantoms mimicking human vasculatures (e.g. Fig. 5h and Fig. 5i) in both non-pulsatile and realistic pulsatile flow conditions.

6.2. Method for Level 2 Platform Assessment

Here, a special experimental set-up was developed to validate the mathematical models and related hypotheses for much smaller untethered entities. A smaller and simpler prototype of the SGC with the minimum hardware required to investigate the steering capability of smaller particles within realistic technological constraints and physiological conditions was built. It consisted of a Maxwell pair (*dB/dz* = 443mT/m, radius = 0.0603m, 100 turns of Cu square insulated wire AWG 13, max. current = 20A) placed inside the bore of the same MRI system used for the level 1 experiments (Sect. 6.1). This gradient value has been chosen as an approximate realistic maximum gradient level achievable on a SGC having an inner diameter suitable for a human and based on prior calculations and interactions with experts and designers of MRI gradient coils.

Magnetite (Iron Oxide, Fe_3O_4) particles (magnetization saturation approximately four times less than FeCo particles) with a diameter of 10.9µm and chosen to ensure biocompatibility were steered in a Y-shape 100µm diameter microchannel placed between the Maxwell pair. Physiological conditions for blood vessels of equivalent diameter were reproduced including blood flow conditions based on data provided in (Whitmore 1968; Charm and Kurland 1974).

6.3. Method for Level 3 Platform Assessment

Samples from the same culture of MC-1 MTB being grew in our laboratory facilities were first characterized in terms of swimming speeds, thrust forces and controllability in a smaller scale version of the SMC depicted in Fig. 4. The smaller version allowed us to mount the SMC directly under the objectives of a Zeiss Axio-Imager optical microscope. In most experiments, the microscope used an objective LD Epiplan 20× in reflection-mode microscopy using dark-field illumination. A video camera Axiocam MRm from Carl Zeiss was mounted on the optical microscope to record the displacements of the MTB when subjected to various directional fields with intensities varying between 0.5 and 20 Gauss (1mT = 10 Gauss). Microchannels with widths varying from 12µm to 4µm were also fabricated using a special fabrication platform (Bey-Oueslati and Martel 2006) developed in our laboratory. The microchannels were then placed inside the miniature SMC being interfaced to a computer. Solutions containing the MC-1 bacteria were injected in the microchannels with a syringe. A custom tracking and analysis software program (Mankiewicz et al. 2007) linked to the computerized optical microscope was used for real-time tracking and the recording of several parameters and characteristics of the swimming bacteria when subjected to various directional field intensities generated by the SMC. Another set of tests consisted of investigating the capability of the bacteria not only to swim in the microvasculature networks but also to penetrate deeper in the tumor through the interstitial tissue of the tumoral lesion for enhanced targeting and therapeutic efficacy. As such, tumors were growth in rats. Then MC-1 bacteria were injected in the blood vessels of these living rats and magnetic gradients were used to orient the swimming path of the MTB to penetrate the tumor through the interstitial tissue. Upon completion of the experiments, thin slices of the tumors were taken and analyzed under microscope. Different

concentrations of living MC-1 MTB were also placed in the bore of the same clinical MRI system used for the previous tests to investigate and validate the possibility of visualizing and tracking MTB and MTB-tagged carriers and nanorobots deep in the human body using MRI for control purposes.

7. Results and Discussions

The results obtained experimentally with the methods described in Sect. 6 were correlated and plotted to predict the performance of level 1, 2, and 3 of the proposed medical nanorobotic platform. These experimental and extrapolated results between the various configurations of the proposed platform are summarized in Fig. 6 for comparison.

As depicted in Fig. 6, a level 1 platform with maximum gradients from the IGC of 40mT/m assuming a duty cycle R of 50% is better suited for larger untethered entities. Hence, the level 1 platform could support operations in larger diameter blood vessels with the potential of reaching arterioles especially if complementary catheterization or other techniques are used conjointly to reduce or control blood flow in proximity of the arterioles entry points.
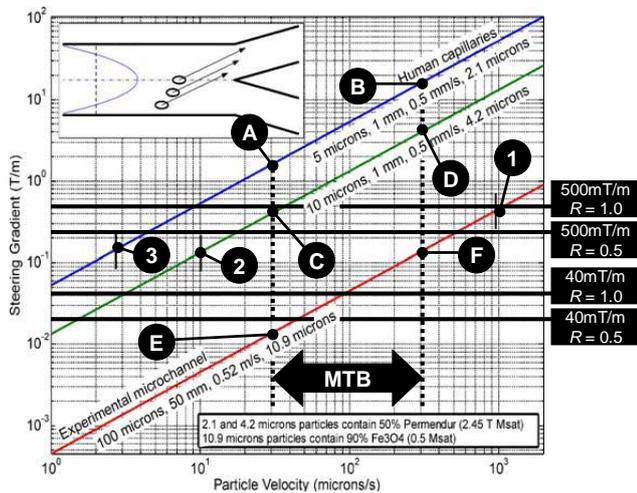

Fig. 6 Results of the three levels of the proposed medical nanorobotic platform - Adapted and upgraded from (Mathieu and Martel 2007). The results show the complementary performance level of each configuration to reach targets through complex microvasculature networks. The data for 2.2μm and 4.2 μm particles with 50% volume Permendur are based on experimental data obtained with particles with a diameter of 10.9μm and 90% volume Magnetite. The graph indicates the diameter of the channel, its length, average velocity of Poiseuille flow from realistic physiological data, and diameter of the particle along each plot for each particle size. Points 1, 2, and 3 show the minimum gradients required for steering the particles at blood vessel bifurcations towards the target while points A through F show initial minimum and maximum velocities of MC-1 MTB-tagged carriers in similar conditions.

The results in Fig. 6 also suggest that a level 2 platform will mostly be essential to operate in the arterioles where the diameters of the blood vessels vary typically between 50-150μm. Possibilities also exist for targeting even deeper in the arteriocapillar networks as depicted by the experimental results obtained with the 10.9μm 90% vol. Magnetite particles (relatively low magnetizatiom saturation of 0.5T) obtained under the experimental conditions described in Sect. 6.2. As depicted in Fig. 6, a SMC assembly providing gradients of 500mT/m with 100% duty cycle ($R = 1.0$) would provided enough force to steer the same 10.9 μm particles at bifurcations towards the target. Although a $R = 1.0$ could not be maintained for a very long time considering that time must be dedicated to tracking and potentially allowing for cooling of the coils, the particles can also be slightly modified to allow efficient steering in these regions while lowering R accordingly. For instance, larger (at least twice the diameter) particles for target embolization or other purposes containing a larger quantity of Magnetite and/or material with higher magnetization saturation can be used.

The potential advantages of a level 3 upgrade are also demonstrated in the results of Fig. 6 when compared against the data for the smaller particles in capillaries interpolated from mathematical models validated with the experimental results obtained with the 10.9μm particles. It shows a clear advantage of using these MTB in the smaller capillaries found in human. Considering our previous results of swimming speeds distribution in human blood of MC-1 MTB ranging from a minimum of 30μm/s to a maximum value of 300μm/s, suggested that even without a pre-selection process of the fastest MTB in the samples, targeting efficacy is expected to be much superior when looking at the distance between point A and point 3 in Fig. 6 representing the lower expected performance level of the MTB in 5μm diameter capillaries and the minimum performance level required for steering at vessel bifurcations to reach a target. In fact, although the results show that particles containing 50% volume of material with the highest magnetization saturation can be steered adequately with SGC generating 500mT/m with $R = 0.5$, the lower and upper performance of MC-1 MTB-tagged carriers under the same physiological conditions would correspond to a SGC operating at $R = 0.5$ capable of generating gradients close to 2T/m and 20T/m respectively. But from experiments conducted by our group, it was shown that the average swimming speed v_{B37} from a large group of MC-1 MTB (without a pre-selection process) from the same culture, decreases gradually over time t (expressed in minutes up to the maximum lifespan or displacement time of the MTB) in human blood at internal body temperature of 37°C from the initial average swimming speed $v_{MTB} = 187.85$μm/s prior to be injected in blood, according to

$$v_{B37} = 0.09\,t^2 - 8.10\,t + v_{MTB}. \tag{4}$$

Even with such a decrease in velocity caused by the relatively high temperature level of the blood, a level 3 platform with MTB-tagged carriers would remain more effective for at least 40 minutes when operating in the human body than a level 2 level platform equipped with a SGC capable to operate at 500mT/m continuously, i.e. without

interruption. But for longer operations, particularly the ones exceeding one hour, a level 2 platform is presently more attractive. The same holds true for the 10μm in diameter capillaries (although the advantages for MTB-tagged carriers become less significant) but the performance of such MTB-tagged carriers becomes insufficient for larger diameter vessels such as in 100μm vessels (below point 1 in Fig. 6).

The advantage here of using MTB supposes that MTB-tagged carriers are designed to maintain equivalent velocities as the ones achieved with the same unloaded MTB. Several examples of such MTB-tagged carriers have been synthesized by our research group. One example demonstrated the principle aimed at loading fluorescent cell penetrating peptide (FITC-LC-Antennapedia – Anaspec, San Jose, CA) inside MC-1 cell which could be replaced by cytotoxic or radio-active agents. Another MTB-tagged carrier designed by our group relies on ~150nm biodegradable polymeric nanoparticles (that could be loaded with cytotoxic or other agents) attached to the cell of the MC-1 bacterium using specific antibodies that have been developed and tested successfully in our laboratory.
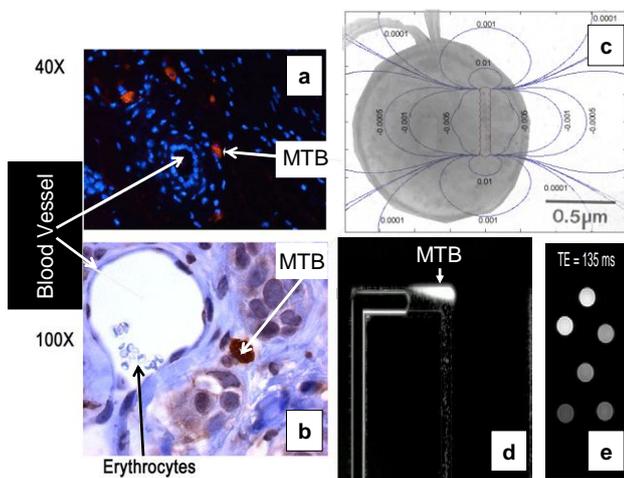

Fig. 7 Results validating the possibility of targeting tumors by controlling magnetotactic bacteria in microvasculature networks; (a) and (b) microscopy images (40× and 100× respectively) of the bacteria after being targeted far in the denser interstitial region of a tumor from the blood vessels; (c) Electron microscopy image of one MC-1 bacterium used for the experiments showing the two flagella and the chain of magnetosomes in the cell with the superposed distortion of the surrounding magnetic field expressed in ppm allowing the bacteria to be tracked deep in human body using MRI; (d) agglomeration of MC-1 bacteria being controlled to swim along pre-determined paths in microchannels mimicking part of the microvasculature and tracked here under an optical microscope; and (e) various concentrations of MC-1 magnetotactic bacteria being detected and imaged with the same clinical MRI system used for the experiments.

The possibility of targeting tumors with MTB in the interstitial region is also demonstrated in Fig. 7a and Fig. 7b. In Fig. 7c, the chain of magnetosomes used for steering

control can also be used for MRI-tracking deep in the human body through a local distortion of the magnetic field inside the bore of the MRI system. The local magnetic field distortion from each magnetosome can be approximated at a point P of coordinate $r(x, y, z)$ by that of a magnetic dipole as

$$\vec{B}'\ P\ = \frac{\mu_0}{4\pi}\left(3\frac{\vec{m}.\vec{r}\ \ \vec{r}}{r^5} - \frac{\vec{m}}{r^3}\right). \qquad (5)$$

where $\mu_0 = 4\pi 10^{-7}$ H·m^{-1} is the permeability of free space such that for a uniformly magnetized object, the dipolar magnetic moment(A·m^2) is given by

$$\vec{m} = \frac{4}{3}\pi a^3 \vec{M}_{SAT} \qquad (6)$$

where a in our particular case is the radius (m) of each Fe_4O_3 magnetosomes (~35nm). This allows an agglomeration of such magnetotactic bacteria such as the one being controlled with a SMC implementation along pre-planned paths in a microchannel as depicted in Fig. 7d to be imaged using MRI as shown in Fig. 7e where different concentration of MC-1 bacteria have been imaged using the clinical MRI platform used for the experiments.

8. Summary and Conclusion

As shown in this paper, the development of a medical nanorobotic interventional platform for operations in the human blood vessels including complex microvasculature networks goes behind the aspect of propulsion alone and must address the integration of many inter-disciplinary components and methods within tight real-time, technological and physiological constraints. Here, such platform with three levels of performance to target deeper in the microvasculature has been proposed and briefly described with results demonstrating the validity of the methods and the platform being proposed. Nonetheless, due to space constraints, many other techniques that can be integrated in this platform to enhance functionality have not been described here. Some examples among many are hyperthermic-based controls and functions making use of focused ultrasound, microwave, and/or radio-frequency being combined with modifications in the design of the carriers for enhanced therapeutic efficacy and remote triggering mechanism for various functions including but not limited to drug releases. Finally, an imaging modality to track the navigable carriers, biosensors, and bacterial nanorobots have been integrated in the proposed platform and validated with a clinical MRI system, allowing closed-loop control of the medical carriers and nanorobots by computer towards destinations that can be located deep in the human body where line of sight is not possible and other imaging modalities become inadequate.

Acknowledgments

References

Alexiou, C., Arnold, W., Klein, R.J., Parak, F.G., Hulin, P., Bergemann C., Erhardt, W., Wagenpfeil, S., and Lübbe, A.S. 2000. Locoregional cancer treatment with magnetic drug targeting. *Cancer Res.*, 60, pp. 6641-6648.

Alexiou, C., Jurgons, R., Schmid, R., Hilpert, A., Bergemann, C., Parak, F., and Iro, H. 2005. *In vitro* and *in vivo* investigations of targeted chemotherapy with magnetics nanoparticles. *J. Magn. Mater.*, 293, pp. 389-393.

Alexiou, C., Diehl, D., Henninger, P., Iro, H., Röckelein, R., Schmidt, W., and Weber, H. 2006. A high gradient magnet for magnetic drug targeting. *IEEE Trans. Appl. Supercond.*, 16(2), pp. 1527-1530.

Behkam, B. and Sitti, M. 2007. Bacterial flagella-based propulsion and on/off motion control of microscale objects. *Appl. Phys. Lett.*, 90, pp. 023902-4.

Bell, D.J., Leutenegger, S. Hammar, K.M., Dong. L.X., and Nelson, B.J. 2007. Flagella-like propulsion for microrobots using a nanocoil and a rotating electromagnetic field. *Proc. of the 2007 IEEE Int. Conf. on Robotics and Automation (ICRA 2007)*, pp. 1128-1133.

Bettmann, M.A, Heeren, T., Greenfield, A., and Goudey, C. 1997. Adverse events with radiographic contrast agents: Results of the SCVIR Contrast Agent Registry. *Radiology*, 203, pp. 611-620.

Bey-Oueslati, R. and Martel, S. 2006. Micro heat pipe fabrication: high performance deposition platform for electronics. *In Proc. 5th Int. Workshop on Microfactories (IWMF)*. Besançon, France.

Charm, S.E. and Kurland, G.S. 1974. *Blood flow and microcirculation*. Wiley, New York, USA.

Chanu, A., Felfoul, O., Beaudoin, G., and Martel, S. 2008. Adapting the software of MRI for the real-time navigation of endovascular untethered ferromagnetic devices. *Magn. Reson. in Med.*, **pp. …**

Ergeneman, O., Dogangil, G., Kummer, M.P., Abbott, J.J., Nazeeruddin, M.K., and Nelson, B.J. 2008. A magnetically controlled wireless optical oxygen sensor for intraocular measurements. *IEEE Sensors J.*, 8(1), pp. 29-37.

Felfoul, O., Mathieu, J.-B., Beaudoin, G., and Martel, S. 2008. MR-tracking based on magnetic signature selective excitation. *IEEE Trans. on Med. Imag.*, 27(1), pp. 28-35.

Fidleris, V. and Whitmore, R.L. 1961. Experimental determination of the wall effect for spheres falling axially in cylinder vessels. *Br. J. Appl. Phys.*, 12, pp. 490-494.

Hatch, G.P. and Stelter, R.E. 2001. **TITLE.** *J. Magn. Magn. Mater.* 225. pp. 262-**???**

Honda, T., Arai, K., and Ishiyama, K. 1999. Effect on micro machine shape on swimming properties of the spiral-type magnetic micro-machine. *IEEE Trans. on Magnetics,* 35, pp. 3688-3690.

Josephson, L., Perez, J.M., and Weissleder, R. 2001. Magnetic nanosensors for the detection of oligonucleotide sequences. *Angew. Chem. Int. Ed.*, 40, pp. 3204-3206.

Li, W.H., Fraser, S.E., and Meade, T.J. 1999. A calcium-sensitive magnetic resonance imaging contrast agent. *J. Am. Chem. Soc.* 121, pp. 1413-1414.

Li, W.H., Parigi, G., Fragai, M., Luchinat, C., and Meade, T.J. 2002. Mechanistic studies of a calcium-dependent MRI contrast agent. *Inorg. Chem.* 41, pp. 4018-4024.

Louie, A.Y., Huber, M.M., Ahrens, E.T., Rothbacher, U., Moats, R., Jacobs, R.E., Fraser, S.E., and Meade, T.J. 2000. In vivo visualization of gene expression using magnetic resonance imaging. *Nat. Biotechnol.* 18, pp. 321-325.

Lowe, M.P., Parker, D., Reany, O., Aime, S., Botta, M., Castellano, G., Gianalio, E., and Pagliarin, R. 2001. pH-dependent modulation of relaxivity and luminescence in macrocyclic gadolinium and europium complexes based on reversible intramolecular sulfonamide ligation. *J. Am. Chem. Soc.*, 123, pp. 7601-7609.

Mankiewicz, M., Mohammadi M., and Martel, S. 2007. Motion tracking and analysis system for magnetotactic bacteria. *In Proc. Int. Symp. On Optomechatronic Technologies (ISOT)*. Lausane, Switzerland.

Martel, S., Mathieu, J-B., Felfoul, O., Macicior, H., Beaudoin, G., Soulez, G., and Yahia, L'H. 2004. Adapting MRI systems to propel and guide microdevices in the human blood circulatory system. *Proc. of the 26th Annual Int. Conf. of the IEEE Eng. in Med. and Biol. Soc.*, San Francisco, USA, pp. 1044-1047.

Martel, S. 2005. Method and system for controlling micro-objects or micro-particles. *US Pat. Appl. 11/145,007.*

Martel, S. 2006a. Controlled bacterial micro-actuation. *In Proc. of the Int. Conf. on Microtech. in Med. and Biol. (MMB)*, Okinawa, Japan.

Martel, S. 2006b. Targeted delivery of therapeutic agents with controlled bacterial carriers in the human blood vessels. *2nd ASM/IEEE EMBS Conf. on Bio, Micro and Nanosystems*, San Francisco, USA.

Martel, S., Tremblay, C., Ngakeng, S., and Langlois, G. 2006. Controlled manipulation and actuation of micro-objects with magnetotactic bacteria. *Appl. Phys. Lett.*, 89, pp. 233804-6.

Martel, S. 2007. Magnetic resonance propulsion, control, and tracking at 24 Hz of an untethered device in the carotid artery of a living animal: an important step in the development of medical micro- and nanorobots. *In Proc. of the 29th Annual Int. Conf. of the IEEE Eng. in Med. and Biol. Soc. (EMBS)*, Lyon, France.

Martel, S., Mathieu, J.-B., Felfoul, O., Chanu, A., Aboussouan, É., Tamaz, S., Pouponneau, P., Beaudoin, G., Soulez, G., Yahia, L'H., and Mankiewicz, M. 2007a. Automatic navigation of an untethered device in the artery of a living animal using a conventional clinical magnetic resonance imaging system. *Appl. Phys. Lett.*, 90(11), **pp. …**

Martel, S., Mathieu, J-B., Felfoul, O., Chanu, A., Aboussouan, E., Tamaz, S., Pouponneau, P., Yahia, L'H., Beaudoin, G., Soulez, G., and Mankiewicz, M. 2007b. Medical and technical protocol for automatic navigation of wireless devices in the carotid artery of a living swine using a standard clinical MRI system. *10th Int. Conf. on Med. Image Computing and Computer Assisted Intervention (MICCAI 2007),* Brisbane, Australia.

Mathieu, J.-B., Beaudoin, G., and Martel, S. 2006. Method of propulsion of a ferromagnetic core in the cardiovascular system through magnetic gradients generated by an MRI system. IEEE Trans. on Biomed. Eng., 53(2), pp. 292-299.

Mathieu, J.-B. and Martel, S. 2007. *In vivo* validation of a propulsion method for untethered medical microrobots using a clinical magnetic resonance imaging system. *In Proc. of the EEE/RSJ Int. Conf. on Intelligent Robots and Systems (IROS)*. San Diego, CA, USA.

Meade, T.J., Taylor, A.K., and Bull, S.R. 2003. New magnetic resonance contrast agents as biochemical reporters. *Curr. Opin. Neurobiol.* 13, pp. 597-602.

Mykhaylyk, O., Dudchenko, N., and Dudchenko, A. 2005. **TITLE HERE**. *J. Magn. Magn. Mater.* 293(1), pp. 473-482.

Seldinger, S.I. 1953. Catheter replacement of the needle in percutaneous arteriography; a new technique. *Acta Radiol.*, 39, pp. 368-376.

Steager, E., Kim, C-B., Patel, J., Bith, S., Naik, C., Reber, L., and Kim, M.J. 2007. Control of microfabricated structures powered by flagellated bacteria using phototaxis. *Appl. Phys. Lett.*, 90, pp. 263901-3.

Tamaz, S., Chanu, A., Mathieu J.-B., Gourdeau R., and Martel, S. 2008. Real-time MRI-based control of a ferromagnetic core for endovascular navigation. *IEEE Trans. on Biomed. Eng*., **pp. …**

Whitmore, R.L. 1968. *Rheology of the circulation*. Pergamon, New York, USA.

Appendix A: Index to Multimedia Extensions

Extension	Type	Description
1	Video	???
2	Video	Directional control by computer of a swarm of MC-1 magnetotactic bacteria in a microchannel